JOURNAL OF MATERIALS SCIENCE 31 (1996) 3747–3761

Styrenics materials and cyclopentane: problems and perspectives

C. MAESTRINI*, A. CALLAIOLI, M. ROSSI, R. BERTANI
Enichem Research Centre, Via Taliercio 14, 46100 Mantova, Italy

The use of chlorofluorocarbons (CFC) and hydrochlorofluorocarbons (HCFC) has been greatly limited in recent years because of their high ozone depletion potential (ODP) (Montreal protocol). The manufacturers of refrigerators have tried various new blowing agents for polyurethane (PU) foams used as insulating panels, and currently the chosen organic compound in Europe seems to be cyclopentane (CP), due to its acceptable insulating power and null ODP and toxicity. Unfortunately the interaction of CP with high impact polystyrene (HIPS) panels of the refrigerators produces blisters and can possibly induce environmental stress cracking (ESC). The aim of this work is, then, to explain the growth of blisters with a theoretical calculation and also to investigate the mechanical behaviour of HIPS in contact with gaseous and liquid CP, in comparison with usually used Freon® 11 (F11).

By means of the group contribution one can calculate with the Flory–Huggins equation an isothermal adsorption curve for the polystyrene (PS) matrix/organic system and with the Chow equation calculate the lowering of T_g. From the calculation it is evident that the lower CP vapour pressure causes a considerable absorption, and this is simultaneous to the lesser CP amount needed to reach a 23 °C T_g for the PS matrix: it is then possible to state that the blisters form from a sort of micro blow-moulding, induced in the plasticized PS by the thermal treatments that are introduced in the refrigerator production cycle. The use of small amounts of acrylonitrile (AN) in the PS matrix may be sufficient to avoid this inconvenience, as it has been confirmed by lab and industrial experiences.

From a mechanical point of view two experimental set-ups were designed in order to evaluate the ESC resistance in gaseous and liquid environment: for the first case slow crack propagation (SCP) experiments were performed in controlled atmospheres on compact tension (CT) specimens, while in the second case the essential work of fracture (EWF) technique was applied to double edge notch (DEN) specimens fully immersed in the considered liquids at different temperatures. In the first case it can be immediately concluded that the ESC produced in the presence of the same pressure of the two different agents (CP and F11) is very different, the CP one being much more aggressive than the F11. However, if the data are plotted versus the thermodynamic activity, there is no meaningful difference between CP and F11, suggesting that this parameter controls the ESC in gaseous environment for the considered blowing agents. In the case of ESC in the presence of a liquid, that could have a practical relevance in refrigerators if condensation phenomena take place, one observes that ordinary HIPS becomes rapidly brittle, while an AN modified HIPS maintains an appreciable ductility also in the presence of the liquid solvents.

1. Introduction

The 1987 Montreal protocol and its revised version produced a progressive ban of chlorofluorocarbons (CFC or Freon®) because of their high ozone depletion potential (ODP). Recently, environmental laws have been promulgated across the whole of Europe, which not only limit the usage of CFCs but also modified CFCs (HCFC) which have a lower or null ODP. Furthermore, an important ecolabel, the *Blauwe Engel* (Blue Angel), has been introduced in Germany for those goods that present a very low environmental impact: this initiative has also proved to be a successful marketing tool. As a result, CFCs and HCFCs are now virtually banished from use in Europe as blowing agents for polyurethane (PU) foams that are used to thermo-insulate domestic and industrial refrigerators [1].

* To whom correspondence should be addressed.

0022–2461

The refrigerator manufacturers are now oriented towards the utilization of cyclopentane (CP). This change created problems in the material used for the internal panels of the refrigerators which is usually high impact polystyrene (HIPS). In CP based refrigerators it was often observed that the presence of small, anti-aesthetic *blisters* on the internal surface of the refrigerators (the one in contact with food) were occurring. This effect has called into doubt the continued utilization of HIPS in CP based refrigerators.

The aim of this work is then to investigate the interactions between CP and HIPS, both from theoretical and experimental points of view, with the specific objective of understanding and improving the behaviour of the real system represented by the refrigerator.

2. Background

HIPS is a polymeric material composed of a matrix of polystyrene (PS) and a population of well dispersed, composite particles, whose rubber component is ordinarily crosslinked polybutadiene (PB) (Fig. 1). The main problem that HIPS experienced in Freon® 11 (F11) based refrigerators was environmental stress cracking (ESC). The HIPS panel in a refrigerator is, in fact, subjected to stress of different origins during its service life and can break down more easily due to the chemical aggression. Some papers have appeared in the literature concerning the ESC of HIPS in contact with liquid substances such as oils, alcohols, hydrocarbons [2, 3] and gaseous substances such as fluorocarbons [4–6]. These studies demonstrated that the parameters to work on in order to enhance the ESC resistance were the matrix molecular weight, the rubbery phase content, the rubbery particle size and morphology and the mineral oil level; on the basis of these observations the HIPS producers were able to develop special grades that could withstand the action of F11 and guarantee a good ESC resistance [7–9].

For practical purposes, a routine test protocol for the control of the ESC resistance became an accepted standard in the field: in 1970 the *Arbeits Gemelnschaft KälteIndustrie* (German Association of Refrigerator Producers) adopted the standard known as AGK 31 [10]. The AGK 31 protocol is briefly summarized as follows: strips of HIPS are obtained from manufacturers and are then loaded for a given amount of time in an environment containing a controlled atmosphere (0.5065×10^5 Pa) of F11, a constant flexural deformation and an initial stress which is considered to be of the same order of magnitude as the stress inside a refrigerator, but below the yielding stress (15–20 MPa for ordinary HIPS), are applied. After this phase the strips are removed from the aggressive atmosphere and deformed in tension in a standard testing machine with a constant grips displacement rate. The relative reduction of the elongation at break with respect to unexposed specimens is considered a practical parameter measuring the chemical damage.

This protocol has proved to be very useful due to its simplicity but has, unfortunately, many controversial points. These include:

1. ESC fractures that take place in service are characterized by the fact that the loading, the attack and the fracture are simultaneous and concomitant, whilst the AGK 31 protocol introduces an arbitrary separation between the phase of the attack and the loading and the phase of the fracture,
2. the temperature of the test (room temperature) is quite far from the service temperatures. In service conditions it is very probable that local condensation of F11 can take place, the boiling point of F11 being about 24 °C (see Table I), giving rise to localized intense HIPS solubilization phenomena which are not accounted for by the AGK 31 test,
3. the elongation at break in a specimen without a notch is a very questionable parameter: in this case, in fact, the fracture always originates from accidental weak spots (dust particles, local inhomogeneities, etc.) that exist inside the material and act as stress concentrators, possibly producing enormous experimental scattering,
4. the choice of a relaxing stress does not seem to fit in a realistic way the stress conditions that can take place in a refrigerator. Furthermore the chosen stress value could be possibly too low, considering the fact that in correspondence of critical points,

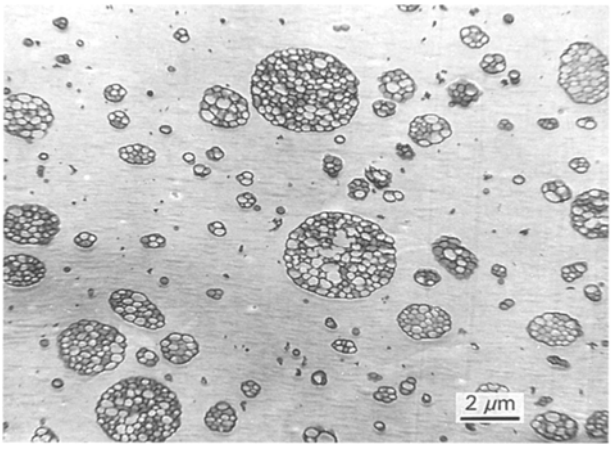

Figure 1 TEM picture of a typical HIPS: the light regions represent the PS matrix, whilst the dark, circular regions represent the PB composite particles.

TABLE I Physico–chemical characteristics of the considered PU blowing agents. CP is from EniChem SpA and F11 from Ausimont SpA

		Cyclopentane	Freon®11
Purity	(%)	99.2	99.7
Molecular weight	($g\,mol^{-1}$)	70.134	137.368
Density (23 °C)	($g\,cm^{-3}$)	0.752	1.482
Molar volume (23 °C)	($cm^3\,mol^{-1}$)	93.239	92.710
Boiling point	(°C)	49.25	23.82
Vapour pressure (23 °C)	($\times 10^2$ Pa)	389	991
Vapour pressure (0 °C)	($\times 10^2$ Pa)	141	401
Vapour pressure (−23 °C)	($\times 10^2$ Pa)	41	133

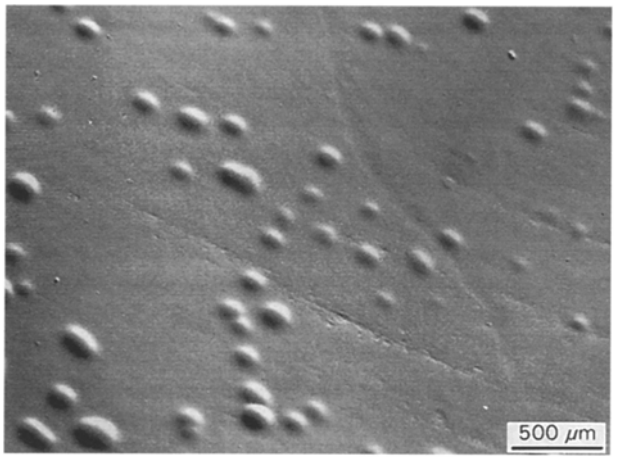

Figure 2 SEM picture of blisters on the inner surface of a HIPS panel in a CP based refrigerator.

like edges, the material can undergo a stress higher than the yielding one.

For these reasons the extension of the AGK 31 protocol to different aggressive agents does not seem to be applicable, taking also into account that in the specific case of CP the vapour pressure is lower than 0.5065×10^5 Pa at ambient conditions.

On the other hand, CP based refrigerators present problems that only rarely occurred when the PU blowing agent was F11: for example the appearance of blisters (Fig. 2), which whilst not necessarily inducing observable fractures, constitute an aesthetic drawback that can result in the rejection of the produced piece, with the consequence of a considerable loss of profit.

The present work will be, then, divided into two parts; the first of which considers the occurrence of the blisters and advances an explaining hypothesis based on theoretical calculations, and the second one proposing and studying some methods, different from the AGK 31, for the characterization of the ESC resistance of HIPS in CP in comparison with the traditional blowing agent, F11.

3. Surface damage (blistering)

Zanussi Inc. and Whirlpool Inc., major European producers of refrigerators, provided some interesting observations concerning the frequent occurrence of blisters in refrigerators prepared using CP based PU [11]. The blisters do not form immediately after the filling of the refrigerator doors with the PU foam, but mostly after a heating treatment at a temperature of about 60 °C, introduced in the production process in order to simulate storing periods at elevated temperatures. As we said before, the phenomenon of blistering occurred very rarely with F11 based PU.

In order to explain the phenomenon it is necessary to have a more precise idea of a refrigerator panel: Fig. 3 is a useful schematic representation. In every cell of the PU foam there will be a given concentration and consequently a given pressure of the blowing agent. The blowing agent, which ordinarily is a small organic molecule, has the tendency to dissolve into the

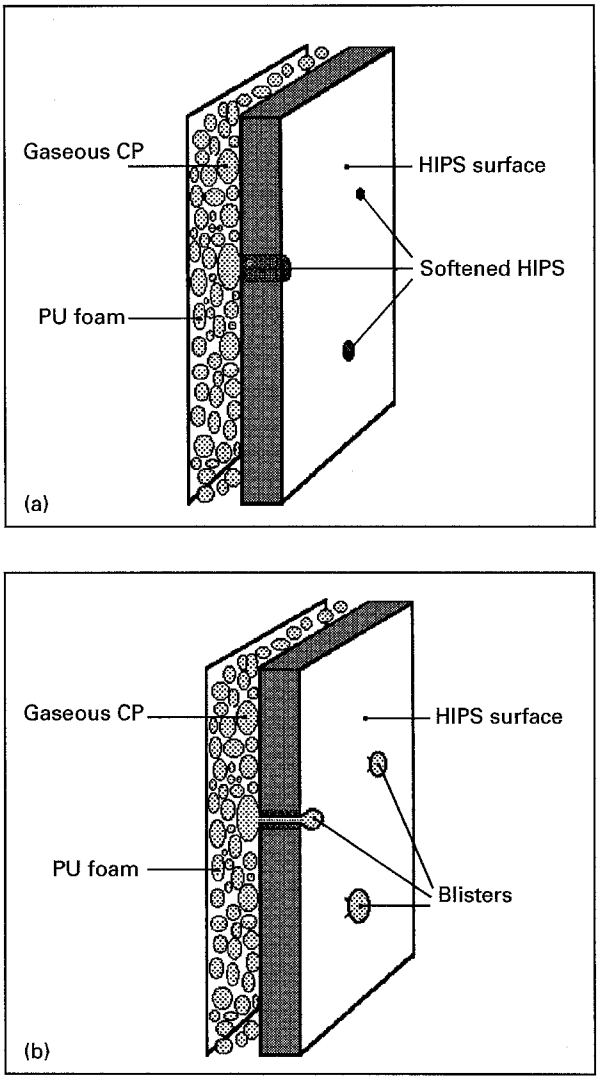

Figure 3 Scheme of the refrigerator panel. Mechanism of blister formation: (a) plasticization; (b) formation of the blisters.

polymeric material forming the panel. In order to simplify the problem we will consider in the following discussion only the interaction with the PS matrix, neglecting the rubbery phase contribution. The degree of affinity between the polymer and the vapour can be expressed by means of a parameter known as the Flory–Huggins interaction parameter [12], χ, composed of two contributions:

$$\chi = \chi_s + \chi_h, \tag{1}$$

where χ_s represents an entropic part, which does not change very much and has a value that for the great majority of polymer–solvent systems is on the order of 0.3–0.4 [13], and χ_h is an enthalpic part, that for non-polar, non-hydrogen bonding polymer–solvent systems is given by [14]:

$$\chi_h = \frac{V_s}{RT}\left(\delta_P - \delta_s\right)^2, \tag{2}$$

where V_s is the solvent molar volume, R the universal gas constant, T the absolute temperature and δ_P and δ_s the Hildebrand solubility parameters for the polymer and the solvent, respectively.

A knowledge of the interaction parameter is extremely helpful. In fact, by means of the Flory–Huggins equation for the thermodynamic activity, α, defined as the ratio between the solvent pressure at the equilibrium with the polymeric solution (P), over the vapour pressure of the pure solvent at the same temperature (P_0):

$$\ln\alpha = \ln\frac{P}{P_0} = \ln\phi_s + \phi_P + \chi\phi_P^2, \qquad (3)$$

where ϕ_s and ϕ_P are the solvent and polymer volume fraction, respectively, and using the formula:

$$\text{weight gain} = \frac{\phi_s d_s}{\phi_P d_P}, \qquad (4)$$

where d_s and d_P are the solvent and polymer density, respectively, we can calculate the weight gain of the polymer. It is possible, at this point, to plot the weight gain of the polymer in contact with the considered organic versus the organic pressure or activity at the thermodynamic equilibrium. Figs 4 and 5 show these plots in the cases of CP and F11.

From an examination of Fig. 4 it is evident that the dissolved amount of CP is always greater than that of F11, due to the fact that the pure solvent vapour pressure at 23 °C is 389×10^2 Pa for CP and 991×10^2 Pa for F11. In fact, the weight gain of the polymer rapidly increases when the pressure approaches the pure solvent vapour pressure. On the other hand, the χ parameter influences the shape of the curves shown in Figs 4 and 5. Furthermore, we can note that, considering the activity instead of the pressure (Fig. 5), the difference between CP and F11 is not so remarkable: we will come back on this evidence later in this paper.

When a polymer is in contact with a solvent and is plasticized the system glass transition temperature (T_g) lowers: this decrease in T_g can be computed knowing the molar volume of the solvent and some physico–chemical parameters of the polymer [15, 16]. In order to reduce the T_g of the system to 23 °C, making it soft at room temperature, a weight gain of about 12% for CP and 23% for F11 is needed. Taking into account the above mentioned considerations, it is very likely that the effective T_g of the system should be lower when the material is in contact with a CP based PU foam, than with a F11 based foam.

The blistering occurrence can now be understood: when the temperature of the system increases from room temperature, as happens during the industrial heating treatments, the blowing agent pressure will increase accordingly. If the polymer is softened enough by the solvent, it cannot bear the stress and will be swollen, in a sort of *micro-blow-moulding* process, producing in this way the bubble that will initiate the blister (Fig. 3). It is also possible that the pressure can reach values high enough to cause the melt fracture of the blister, yielding in this way to the small holes that have often been observed, together with the bubbles, in the refrigerators.

Despite the fact that it accounts for the difference observed in the surface damage for CP and F11 based

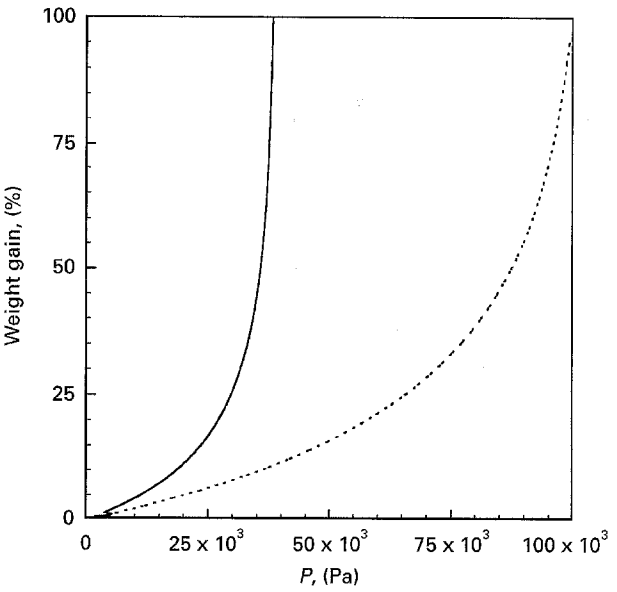

Figure 4 Plot of the PS weight gain at the thermodynamic equilibrium versus the pressure for CP (solid line) and F11 (dotted line); $T = +23$ °C.

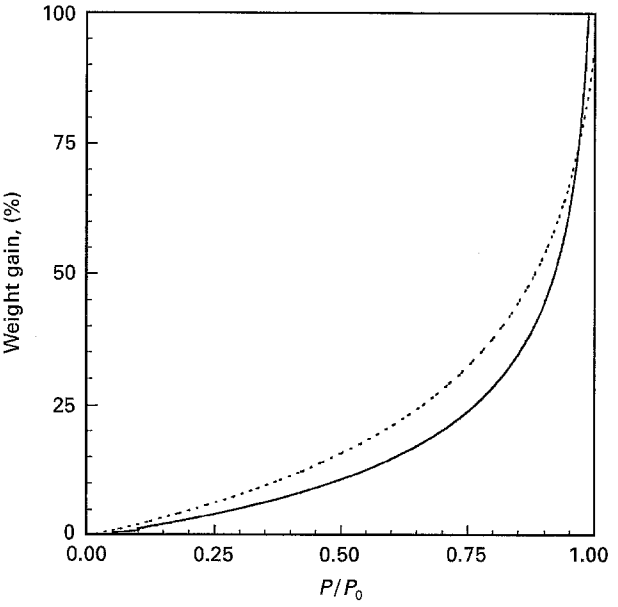

Figure 5 Plot of the PS weight gain at the thermodynamic equilibrium versus the thermodynamic activity for CP (solid line) and F11 (dotted line); $T = +23$ °C.

refrigerators, the above outlined model has, of course, to be intended only as a rough description. In the model, for example, we assumed no contribution from the rubbery dispersed phase contained in the material composing the refrigerator panel, that, on the contrary, can play a role on the blistering phenomenon. Nonetheless the model suggests some possible strategies to avoid the occurrence of the bubbles, that can be usefully applied in the production of refrigerators. First of all, and this is the road followed at the present moment by many refrigerator producers, one can use, instead of ordinary HIPS, a material chemically modified, in which a small amount of acrylonitrile (AN) is added to the PS polymer chain. In this way the affinity between the polymer and the solvent is lower and consequently the weight gain and the T_g decrease are

reduced. In this case one can probably count also on a lower diffusivity inside the polymer, making the thermodynamic equilibrium more difficult to reach. As a matter of fact, the introduction of a quantity of about 8% of AN in the matrix has proved to be sufficient to completely eliminate the occurrence of blisters.

On the other hand, it is also possible to modify the PU foams: in fact a large number of blisters were observed in non-homogeneous regions of the PU foam, inside which one can assume a higher concentration of the blowing agent. Consequently, if a CP based foam could be produced with a more uniform foam distribution and reduced residual pressure in the cells, within the obvious constraint of a good thermal insulation,† it is conceivable that the phenomenon of blistering could diminish or even disappear. Finally, if the storage temperature is kept low the probability of inducing the hypothesized mechanism of micro-blow-moulding could also be greatly reduced.

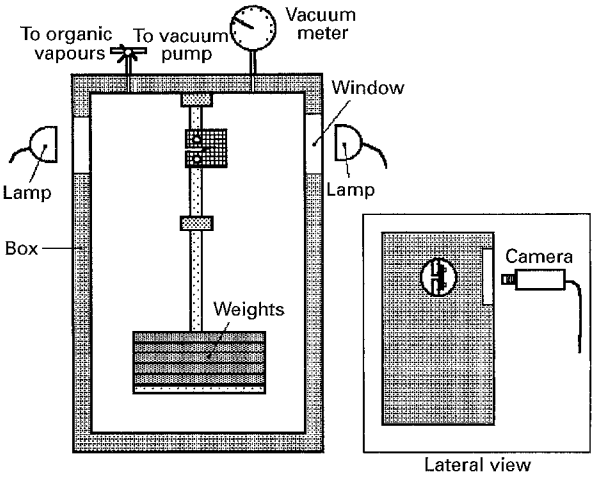

Figure 6 Scheme of the experimental set-up used for ESC experiments in a gaseous environment.

4. Experimental

4.1. Environmental stress cracking

The analysis of the weakness of the AGK 31 test suggest some ideas that can be profitably used to develop better methods for the ESC resistance characterization in the refrigerator field. The methods should:

1. reproduce realistic aggressive conditions in which the chemical aggression, the load and the fracture take place *simultaneously*;
2. be able to explore widely different experimental conditions, in terms, for example, of stress and temperature; they should also be able to investigate the difference existing between an aggression taking place in a liquid and in a gaseous environment;
3. involve intrinsic mechanical parameters, supporting in this way the knowledge of the aggression phenomena in terms of structure–property relationships.

Concerning this last point it is easy to think of the tools offered by fracture mechanics, and several experimental techniques suitable to our investigation have already been developed and discussed, as we will see in the following discussion. The points 1 and 2, on the contrary, need to be considered more carefully and for them we developed *ad hoc* solutions. In the following part of the present paper we will, then, describe our attempts, dividing the presentation in two parts, the first one concerning ESC in a gaseous environment, and the second for a liquid environment.

4.1.1. ESC in a gaseous environment

The usage of gaseous solvents in ordinary modern dynamometers is very risky due to the fact that a chemical attack can damage the complex electronic circuits that control the machines. It is safer, for this purpose, to develop a testing equipment as simple as possible that could be entirely contained in a sealed box inside which the nature and pressure of the atmosphere could be adjusted. In order to avoid the introduction inside the box of load sensors, that can be easily damaged by the solvent, it is more straightforward to test the materials at a constant load, for which case no elaborate measurements are needed.

If the examined samples contain a pre-notch, the crack advance can be easily examined also if the applied load is constant, because of the fact that the stress conditions at the crack tip, described by the *stress intensity factor*, K, changes with changing the crack depth. It is possible, in this way, to examine the *sub-critical* or slow crack propagation (SCP) regime, which is a phase of the fracture that is very interesting from the practical point of view.

These considerations brought us to the development of the equipment sketched in Fig. 6. The box is designed to sustain internal pressures lower than 1 atmosphere (1.013×10^5 Pa) and the internal temperature can be varied in the range -10–$+50$ °C. The maximum permitted load on the creep support inside the box is about 40 kg, while the circular windows have the function of allowing the observation of the crack advance during the test. The box is also provided with an efficient electrical grounding system to avoid the accumulation of electrostatic charges and the tests in the presence of the solvent have always been performed after an oxygen removal procedure in order to avoid explosions.

We adopted compact tension (CT) specimens, machined from compression moulded plates, containing a sharp (razor made) notch; the specimen dimensions are reported in Fig. 7. They are quite large to permit the observation of the sub-critical crack advance for a length of some mm. The computation of the stress

† A crucial contribution to the thermal insulating power of the PU foam is given by the residual blowing agent. If the foam loses the organic and is filled by air, whose thermal conductivity is much higher, the insulation significantly decreases.

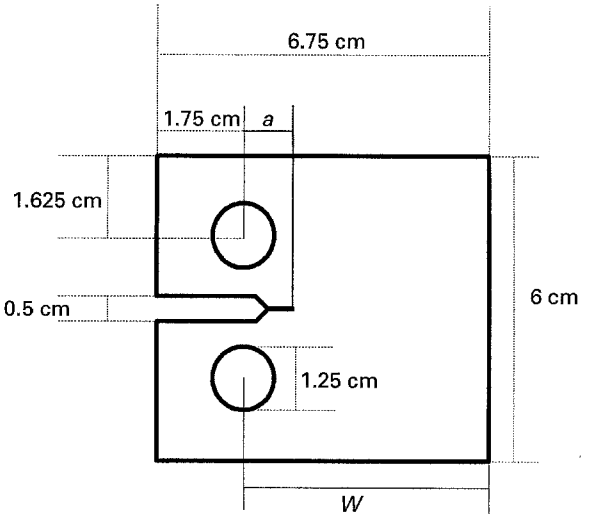

Figure 7 Quoted sketch of the CT specimen used in the slow crack propagation experiments. The considered thickness is 3.2 mm.

intensity factor has been made according to the formula [18, 19]:

$$K = f \times \frac{P}{B \times W^{1/2}}, \tag{5}$$

where P is the applied load, B the specimen thickness, the meaning of W is illustrated in Fig. 7 and f is given by:

$$f = \frac{2 + \frac{a}{W}}{\left(1 - \frac{a}{W}\right)^{3/2}} \left[0.886 + 4.64\frac{a}{W} - 13.32\left(\frac{a}{W}\right)^2 + 14.72\left(\frac{a}{W}\right)^3 - 5.6\left(\frac{a}{W}\right)^4\right], \tag{6}$$

where a represents the fracture coordinate. Equations 5 and 6 hold when $0.2 < a/W < 0.8$: data out of this range were never considered.

A camera with a magnifying objective lenses of about 6× was used in order to follow the fracture advance: such a magnification was sufficient to have a good resolution of the crack tip position. A gold grid sputtered onto the specimen was utilised as a dimensional reference, avoiding complicated calibration for the lenses magnification factor [20]. The camera was mounted on a positioning device that allowed very small displacements, keeping the images still during the motion. The images were recorded onto a VCR. The frames were successively printed by means of a video printer and the values of the fracture coordinate were simply obtained from the pictures. Some preliminary, interrupted experiments demonstrated that, if the specimens were properly aligned, avoiding mode II and III components in the fracture process, and the razor notch was not oblique, the position of the fracture on the side of the specimen, recorded by the VCR, was coincident with the position in the bulk.

For the determination of the crack speed we adopted the following method: generally we observed that the plots of the measured $a(t)$ values versus $\log [1/(t_f - t)]$, where t_f is the total fracture time and

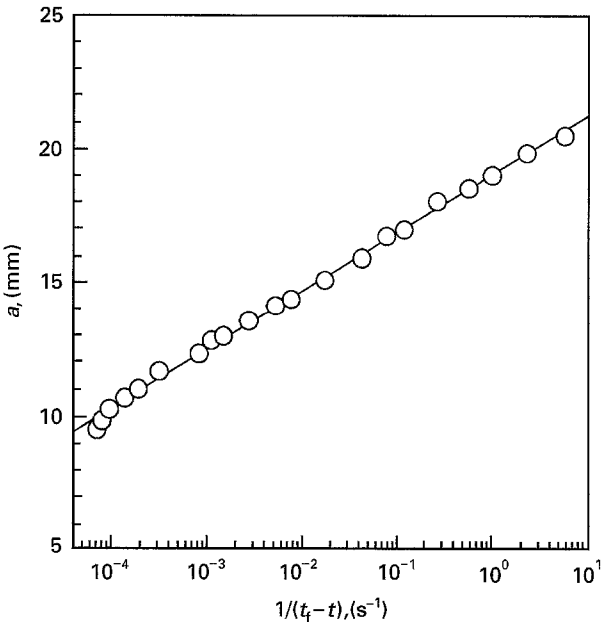

Figure 8 Logarithmic plot of the crack coordinate, a, versus $1/(t_f - t)$ for a specimen of material B fractured in an atmosphere of F11 at 300×10^2 Pa. The solid line represents a linear regression.

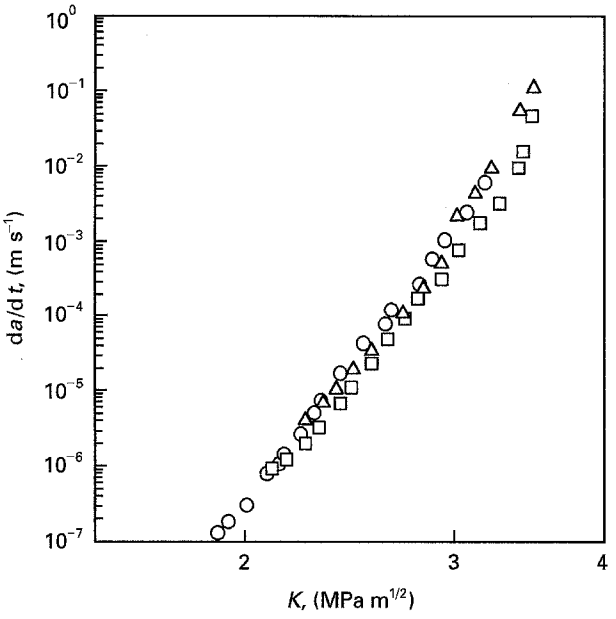

Figure 9 Paris plot for three different specimens (○, □, △) of material B fractured in an atmosphere of F11 at 300×10^2 Pa.

t represents the time coordinate, were well defined straight lines (Fig. 8 is a typical example) [20]. It is possible then to write:

$$a(t) = M + N \log\left(\frac{1}{t_f - t}\right), \tag{7}$$

where M and N are constants that can be obtained from the experimental data relative to each sample. We can immediately conclude, then, that:

$$\frac{da}{dt} = \frac{N}{t_f - t}. \tag{8}$$

Consequently, it was possible to obtain logarithmic plots of da/dt versus K, often designated in the literature as Paris plots [21–23]; Fig. 9 is a typical example

of a Paris plot for the considered materials. It is, in fact, agreed that the phenomenon of sub-critical crack advance is reasonably well described for a wide range of materials, including the great majority of polymers, by the Paris law [21–23]:

$$\frac{da}{dt} = AK^m, \tag{9}$$

where A and m are two phenomenological constants that have to be extracted from the experimental data.

The experimental results will be presented and discussed in the results and discussion part of this work.

4.1.2. ESC in a liquid environment

Some condensation of the PU blowing agent is very likely to occur when the refrigerator temperature is well below room temperature. In principle, the ESC in liquid, due to its extreme intensity, can have different features to that of the ESC in the gaseous atmosphere; it is, therefore, interesting and useful also to examine the ESC resistance in this case.

The chemical attack produced by a liquid solvent generates a strong plasticization in HIPS. In this case it is very difficult to define a stress intensity factor, because the stress–strain behaviour is far from the linear elasticity that the stress intensity factor approach supposes and also notch blunting is relevant from the very first phase of the fracture. Consequently it is hard to adopt the same technique that we described for the ESC in the gaseous atmosphere.

We therefore followed a different approach. Considering the ductility that HIPS shows, we decided to test its mechanical resistance by means of the method known as *essential work of fracture* (EWF). Following the approach pioneered by the groups of Broberg and Cotterell [24–27] that was expanded by Mai and Powell [28] and Paton and Hashemi [29] the plastic fracture problem can be addressed by dividing the zone in which the fracture takes place into two parts: a *final* zone, close to the crack tip, in which the mechanical energy is changed into fracture work, and an *external zone*, in which, the mechanical energy is dissipated by the plastic deformation. This fact gives rise to a sort of crack tip shielding phenomenon, inducing an increase in toughness. The mechanical energy dissipated in the final zone is considered to be an intrinsic property of the material and has received, indeed, the name of essential work of fracture. In order to measure it, it is necessary to divide the two energetic contributions. Let us consider a double edge notched (DEN) specimen (Fig. 10) tested in tension, if we assume that the total fracture work, W_f, can be split into two contributions:

$$W_f = w_e lB + w_P \gamma l^2 B, \tag{10}$$

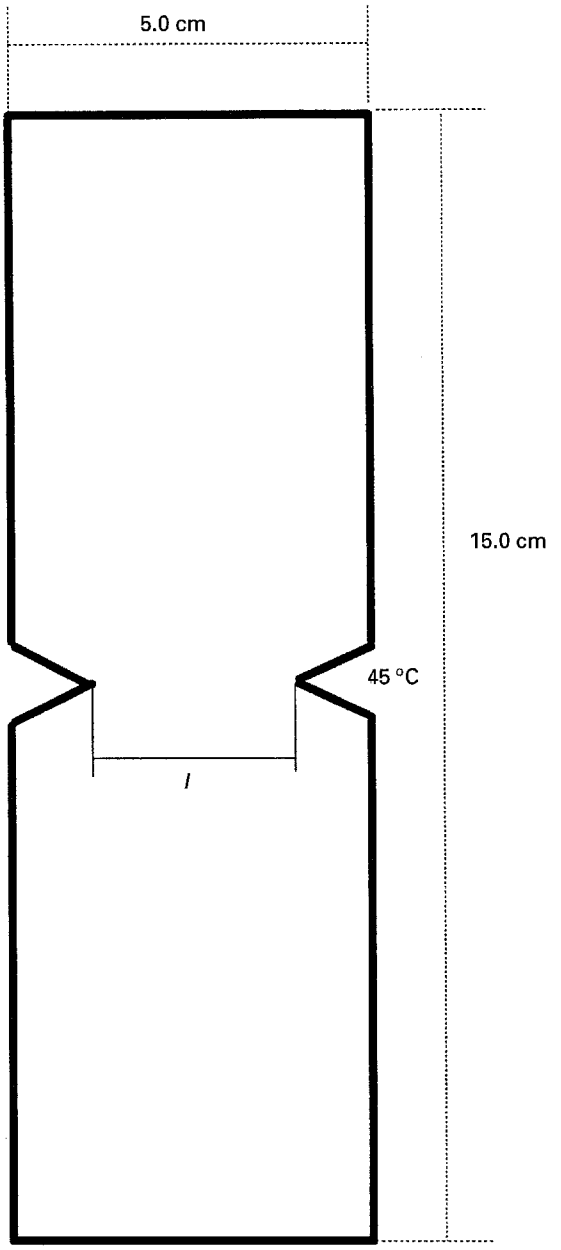

Figure 10 Quoted sketch of the DEN specimen used in the essential work of fracture experiments. The considered thickness is 1 mm.

where B is the specimen thickness, l the ligament, γ a form factor for the plastic zone and w_e and w_P the elastic and plastic energetic contributions, respectively. It is easy to recognize that a plot of $W_f/(lB)$ versus l will have a linear shape and provide the value of the essential work of fracture, w_e, as the intercept of the line interpolating the data,[††] while the slope of the plot will describe the plastic contribution.

Our experimental set-up was then the following: we machined from compression moulded plates, DEN specimens having dimensions as described in Fig. 10 and different ligaments. Razor tips at the notches were produced carefully, using a magnifying lens and a positioner. The specimens were then tested in

[††] Of course there are some assumptions to be made and the approach cannot be followed without checking that some limitations are satisfied: namely that l does not have to be greater than the plastic zone at the crack tip, l does not have to be too big with respect to the total specimen width and l has to be at least five times the specimen thickness, B. A discussion of the details of the EWF approach is, however far from the purposes of the present paper and we refer to the previously mentioned references.

TABLE II Molecular and structural characteristics of the two HIPS materials considered

		HIPS A	HIPS B
Acrylonitrile	(Wt%)	0	8
Polybutadiene	(Wt%)	9	9
Rubbery phase	(Vol%)	35	35
$\langle R^1 \rangle$	(μm)	0.12	0.33
β^2		4.26	1.88
Matrix Mw	($g\,mol^{-1}$)	145000	145000
Young's modulus	(MPa)	1350	1420
Tensile yielding stress	(MPa)	15.0	15.2

tension in the liquid environment, by means of a small glass container fixed to the specimen itself, and at the chosen temperature using an ordinary dynamometer with grip displacement rate of 5 mm per min. From the stress–strain curves it was possible to obtain the value of the fracture energy, while the precise value of the ligament was measured *a posteriori* by means of a metallographic optical microscope. Curves of $W_f/(lB)$ versus l were then easily accessible.

4.2. Materials

In the present work we considered two solvents (reagent grade), CP and F11, and two different HIPS materials. The solvent characteristics are reported in Table I. The main structural and morphological characteristics of the two considered HIPSs are reported in Table II. The choice of the HIPS materials was made in order to match the grades that are now ordinarily used by the refrigerator industry.

The HIPS data are obtained following ordinary characterization methods, with the single exception of the dispersed phase geometric features. In fact, in order to realize a precise and quantitatively useful structural characterization an accurate determination of the particle size distribution and of the dispersed phase volume fraction is necessary, The ordinary way of measuring these two key parameters are, in fact, subjected to some criticism and give rise to data that cannot be considered realistic [31, 32]. For this reason, we adopted the stereological approach described in detail in Ref. [31], that consists in analysing transmission electron microscopy (TEM) pictures, obtained followed the standard technique reported in Ref. [33], from material slices having different thickness and then reconstructing the bulk situation. We used the following equations [31]:

$$\langle r^1 \rangle = \frac{\pi \langle R^2 \rangle + 2t \langle R^1 \rangle}{4\langle R^1 \rangle + 2t}, \tag{11}$$

$$\langle r^2 \rangle = \frac{4\langle R^3 \rangle + 3t \langle R^2 \rangle}{6\langle R^1 \rangle + 3t}, \tag{12}$$

$$\phi_{app} = \frac{4\langle R^3 \rangle + 3t \langle R^2 \rangle}{4\langle R^3 \rangle} \phi, \tag{13}$$

where the $\langle r^i \rangle$ represents the i-th moment of the particle radius distribution in the TEM images, $\langle R^j \rangle$ the j-th moment of the real particle distribution in the bulk, t the observed section thickness, ϕ_{app} the apparent rubbery phase volume fraction in the TEM images and ϕ the real second phase volume fraction. Equations 11–13, which produce an over-determined system when one considers more than one thickness, have been solved using a simple algorithm, which consists of the minimization of the maximum component of a normalized linear error function containing all the parameters $\langle R^j \rangle$ and ϕ. For practical purposes it is useful to define the parameter β:

$$\beta = \left(\frac{\langle R^2 \rangle}{\langle R^1 \rangle^2} - 1 \right)^{1/2}, \tag{14}$$

and representing the dispersion of the distribution, which is the one reported in Table II.

5. Results and discussion

Figs 11–14 contain the Paris plots for the considered materials in the two aggressive agents in the different experimental conditions and Table III summarizes the results. It is clear from the figures that the aggressive atmosphere has a relevant effect that increases the crack speed with increasing the relative pressure.

It has to be pointed out that for samples exposed at 2×10^4 Pa in CP and at 6×10^4 Pa in F11 a relevant plasticization was observed, leading to the blunting of the crack. The corresponding lines in the Paris plot can consequently be incorrect due to the fact that in the presence of a blunt crack the stress intensity factor does not have a precise mathematical meaning. This plasticization phenomenon can be easily understood if we take into account the fact, mentioned in one of the previous sections, that these pressures (2×10^4 Pa CP, 6×10^4 Pa F11) of aggressive agents lower the T_g of the PS matrix down to room temperature.§§

It is interesting now, from the engineering point of view, to confront the crack speed values obtained in correspondence to a defined K value for the materials and the conditions examined. In Fig. 15 we show the crack speed corresponding to a stress intensity factor of 2 MPa $m^{1/2}$ as a function of the pressure of the aggressive agents.

It can be easily seen that the CP is the strongest damaging agent for both materials. Nevertheless material B shows a better performance in air and maintains its superior behaviour up to 2×10^4 Pa for CP and 6×10^4 Pa for F11.

In Fig. 16 we show the same data as a function of the thermodynamic activity of the aggressive agents. In this case we observe that the CP and F11 effects are almost the same for each material, the behaviour of

§§ The calculations presented were relative to the thermodynamic equilibrium conditions. Nonetheless, it is reasonable to assume that these conditions are quickly reached in SCP experiments due to the presence of stress and of damaged material in form of crazes. In fact, considering diffusion rates in the range of 10^{-8}–10^{-12} $cm^2\,s^{-1}$ and a craze fibril diameter of about 25 nm [34], the equilibrium is reached in a time of about 0.1–10 ms, for activities in the experimental range considered in the present paper.

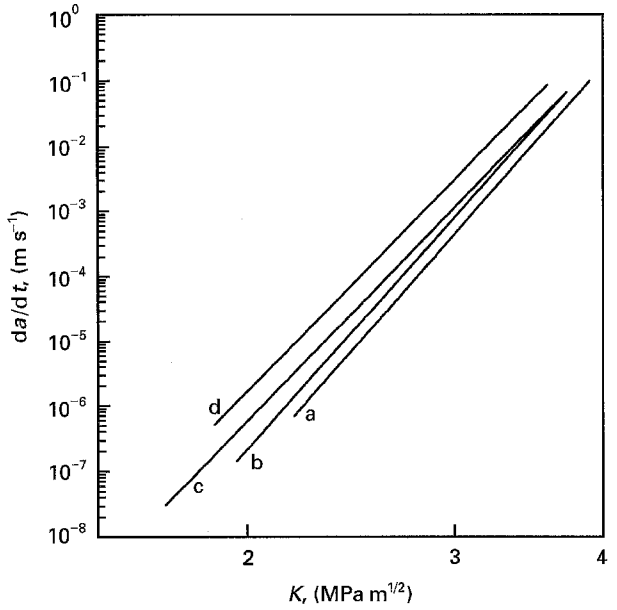

Figure 11 Paris plot for material A. Fractures in (a) air and (b) 100×10^2 Pa, (c) 160×10^2 Pa and (d) 200×10^2 Pa CP atmospheres.

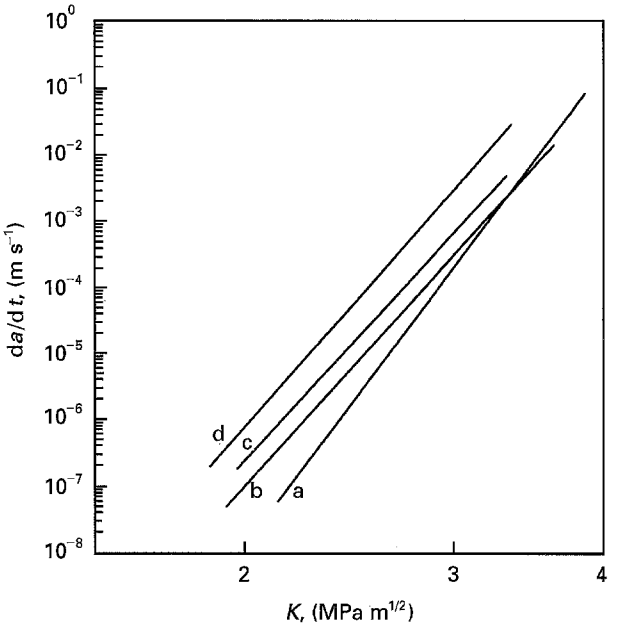

Figure 13 Paris plot for material B. Fractures in (a) air and (b) 100×10^2 Pa, (c) 160×10^2 Pa and (d) 200×10^2 Pa CP atmospheres.

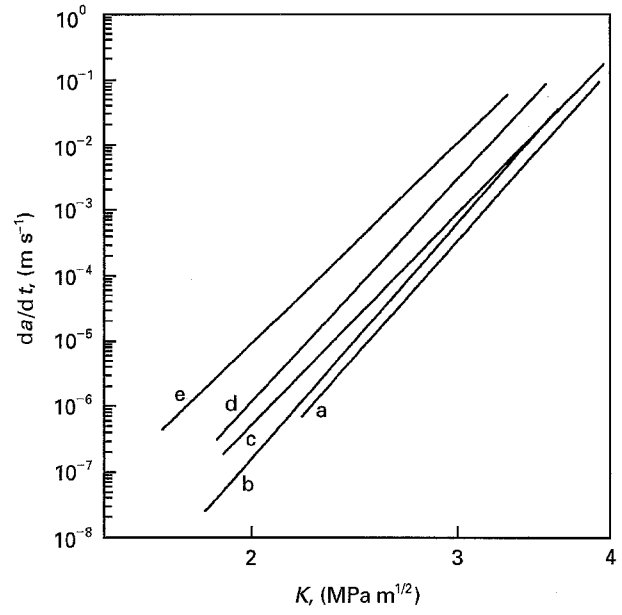

Figure 12 Paris plot for material A. Fractures in (a) air and (b) 160×10^2 Pa, (c) 300×10^2 MPa, (d) 450×10^2 Pa and (e) 600×10^2 Pa F11 atmospheres.

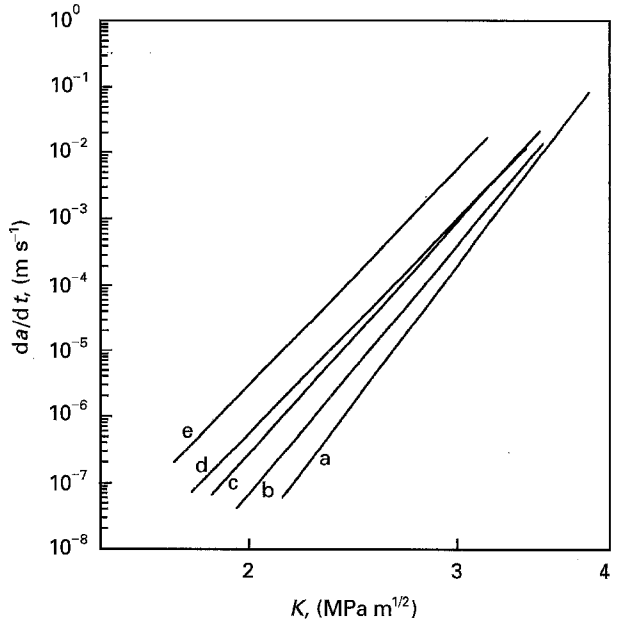

Figure 14 Paris plot for material B. Fractures in (a) air and (b) 160×10^2 Pa, (c) 300×10^2 Pa, (d) 450×10^2 Pa and (e) 600×10^2 Pa F11 atmospheres.

material B being better than that of material A up to an activity of about 0.25. This fact is in agreement with the calculations reported in one of the previous sections concerning the weight gain of the PS matrix as a function of the activity (Figs 4 and 5).

The activity dependence of the crack speed at a given stress intensity factor can, then, be assumed to be the key concept to understand data of SCP in a gaseous aggressive agent, in analogy with data obtained by Olf and Peterlin [35] for polypropylene/He, N_2, Ar, O_2, CO_2 systems, and Brown [36] for poly(chlorotrifluoroethylene)/N_2, CH_4 systems in a range of temperatures from room to the boiling point of the considered gases.

If we assume that in refrigerators F11 and CP are gaseous in the PU foam, differences in the damage of the polymeric panels have to be ascribed to differences in the thermodynamic activity of the aggressive agents.

Considering the experiments performed in liquid environment the results are as follows.

Fig. 17 is a plot of the energy density versus the ligament for material A fractured in air, CP and F11 at +23 °C. This figure shows clearly that the material becomes brittle when in contact with the aggressive agents: the slope of the corresponding curves, in fact, are close to zero, indicating that the energy contribution due to the plastic work is very low. This fact is

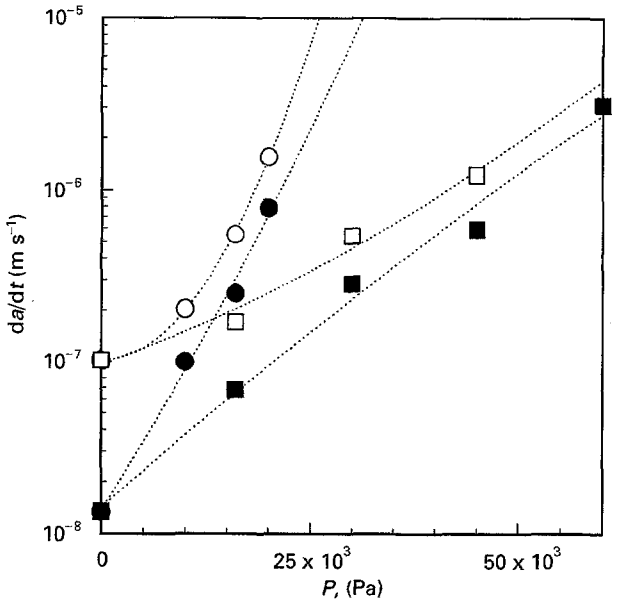

Figure 15 Plot of the crack speed, da/dt, corresponding to a constant value of stress intensity factor ($K = 2$ MPa m$^{1/2}$) versus the pressure, P, for material A (empty symbols) and material B (filled symbols) in CP (circles) and F11 (squares). The dotted lines are simply guides for the eye.

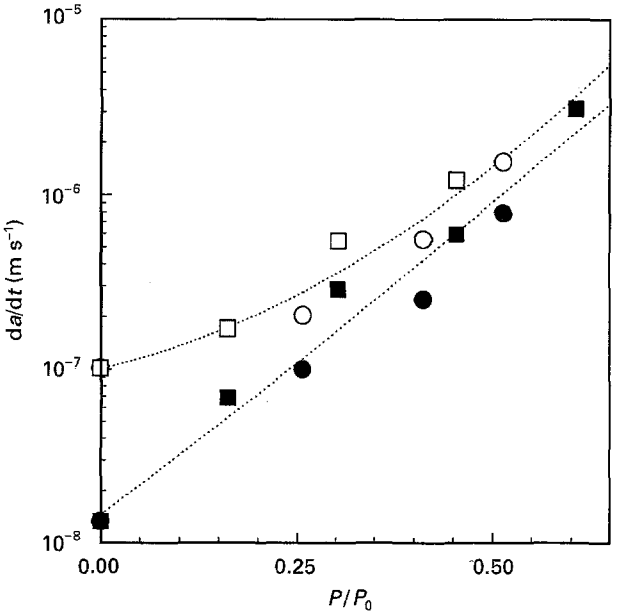

Figure 16 Plot of the crack speed, da/dt, corresponding to a constant value of stress intensity factor ($K = 2$ MPa m$^{1/2}$) versus the thermodynamic activity, P/P_0, for material A (empty symbols) and material B (filled symbols) in CP (circles) and F11 (squares). The dotted lines are simply guides for the eye.

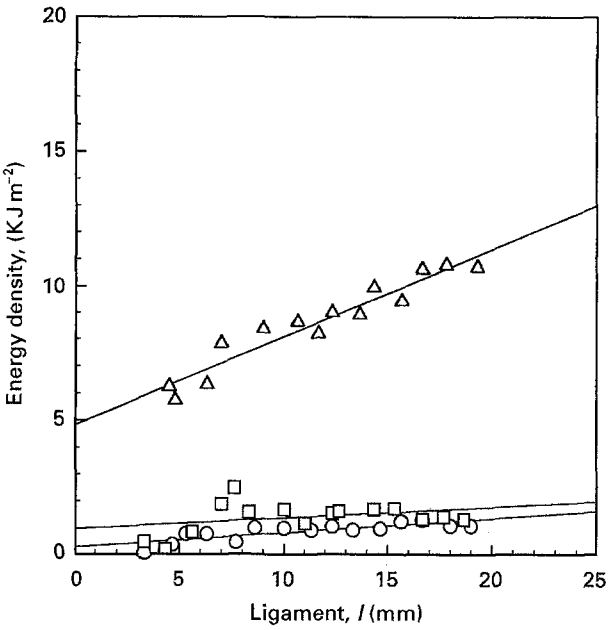

Figure 17 Plot of the energy density, $W_f/(l \times B)$ versus the ligament, l, for material A at a temperature of $+23\,^{\circ}C$ in air (△), in liquid CP (○) and in liquid F11 (□). The solid lines represent linear regressions.

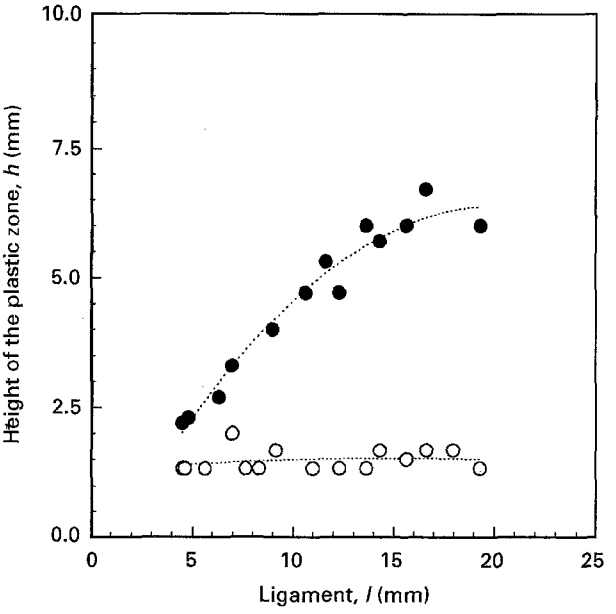

Figure 18 Plot of the height of the plastic zone, h, versus the ligament, l, for material A at $+23\,^{\circ}C$ in air (●) and at $-23\,^{\circ}C$ in air (○). The dotted lines are simply guides for the eye.

confirmed both from the visual inspection and the SEM analysis of the fracture surfaces. The visual inspection of the specimens reveals, in fact, an elliptic plastic zone between the notches that reduces its height as a function of the ligament (as reported in Fig. 18) for the fracture in air, but no plastic zone is observed for the exposed specimens. On the other hand the SEM micrographs of the fracture surfaces (Figs 19–21) show that the attack of the solvents on the upper half of the specimen is very strong, with a complete washing away of the surface itself, which exhibits holes, coming from the evaporation of the solvent.

Fig. 22 is a plot of the energy density versus the ligament for material A fractured in air, CP and F11 at $-23\,^{\circ}C$. An examination of the figure shows that, while the slope of the specimen fractured in air is again positive, testifying to the presence of an active plastic mechanism, the lines that relate to fracture in the liquid agents have, on the other hand, slopes close to zero, indicating fragility, but, in this case, the average value of the fracture energy density appears undeniably higher for CP. The SEM analysis (Figs 23–25) confirms this fact: the attack of F11 is still strong, whilst that of CP may be defined as medium and

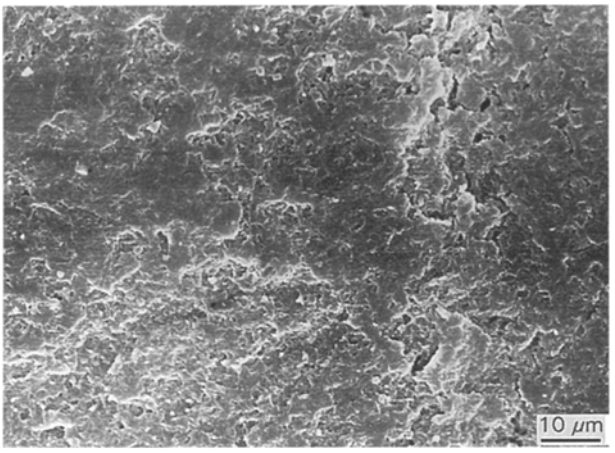

Figure 19 SEM micrograph of the fracture surface of material A fractured in air at +23 °C. The artificial notch is on the right side of the picture, the crack propagates from right to left.

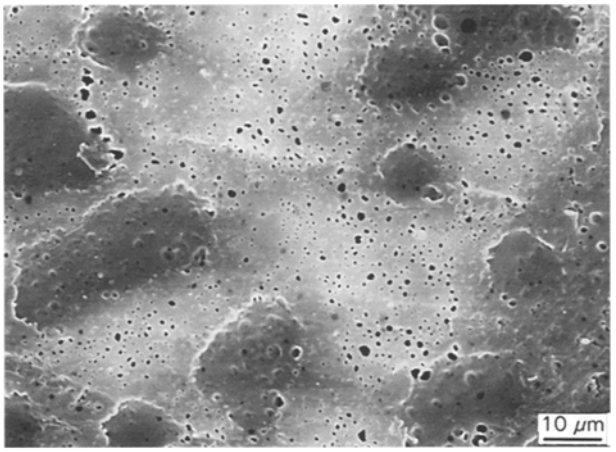

Figure 20 SEM micrograph of the fracture surface of material A fractured in liquid CP at +23 °C. The observed zone is near to the original notch, the crack propagates from right to left.

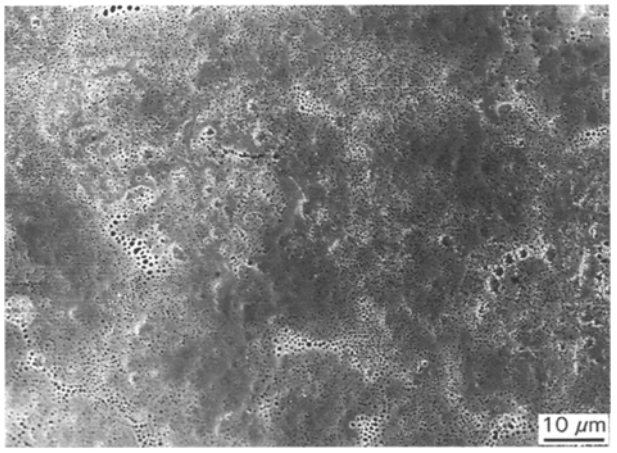

Figure 21 SEM micrograph of the fracture surface of material A fractured in liquid F11 at +23 °C. The observed zone is near to the original notch, the crack propagates from right to left.

without washing away of the surface. It is interesting to note that the presence of the bubbles on the fracture surface (Fig. 25) tends to define the rubbery particles contour: this is due to the fact that the particle boundaries are regions of stress intensification and then of preferential permeation of the solvent.

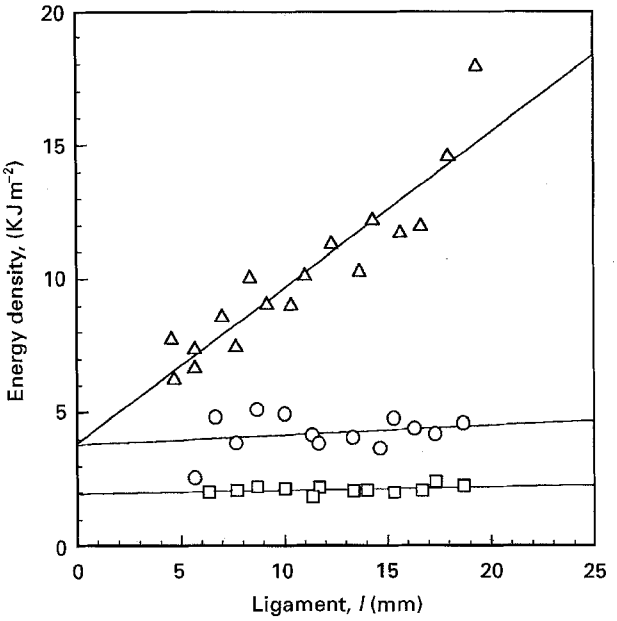

Figure 22 Plot of the energy density, $W_f/(l \times B)$ versus the ligament, l, for material A at a temperature of −23 °C in air (△), in liquid CP (○) and in liquid F11 (□). The solid lines represent linear regressions.

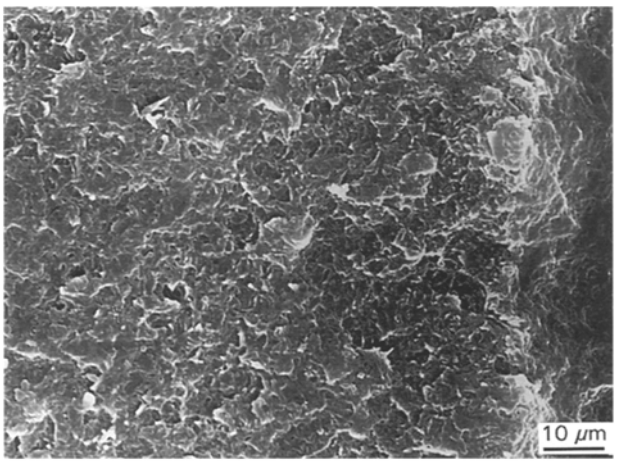

Figure 23 SEM micrograph of the fracture surface of material A fractured in air at −23 °C. The artificial notch is on the right side of the picture, the crack propagates from right to left.

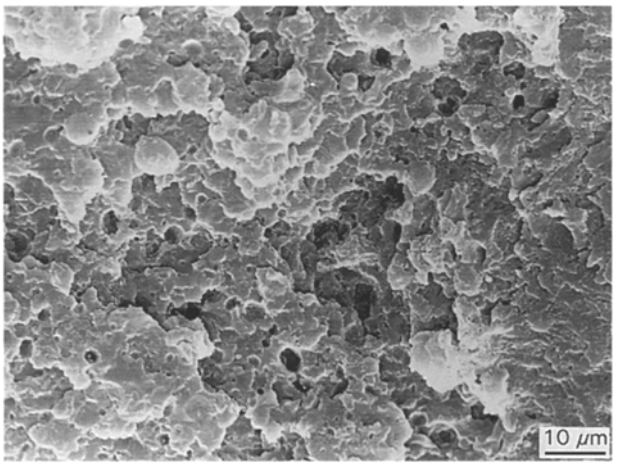

Figure 24 SEM micrograph of the fracture surface of material A fractured in CP at −23 °C. The artificial notch is on the right side of the picture, the crack propagates from right to left.

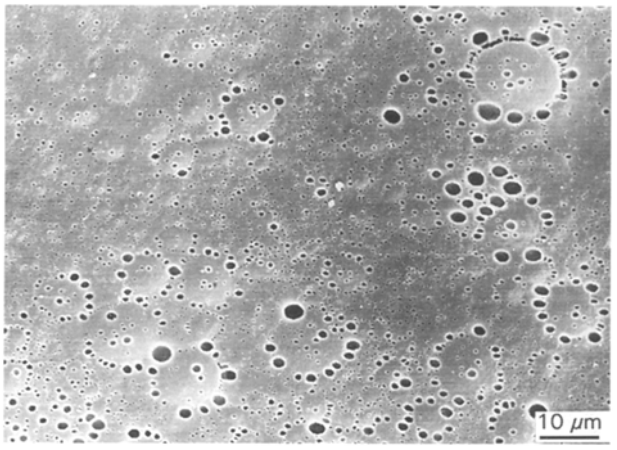

Figure 25 SEM micrograph of the fracture surface of material A fractured in F11 at −23 °C. The observed zone is near to the original notch, the crack propagates from right to left.

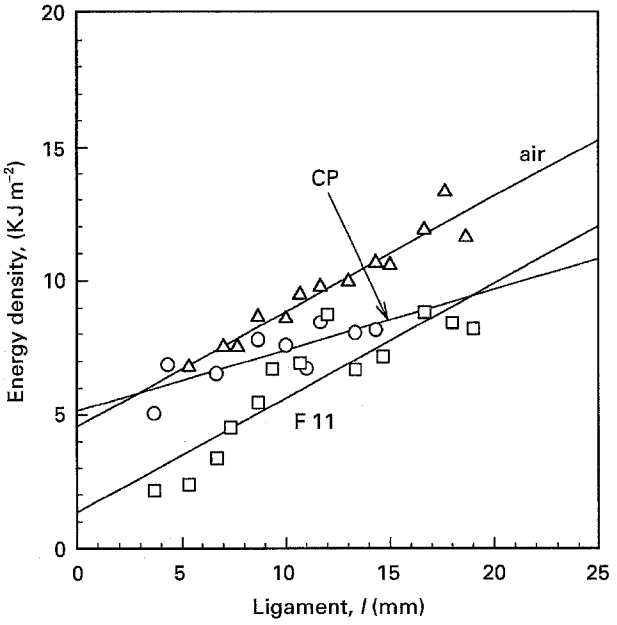

Figure 26 Plot of the energy density, $W_f/(l \times B)$, versus the ligament, l, for material B at a temperature of +23 °C in air (△), in liquid CP (○) and in liquid F11 (□). The solid lines represent linear regressions.

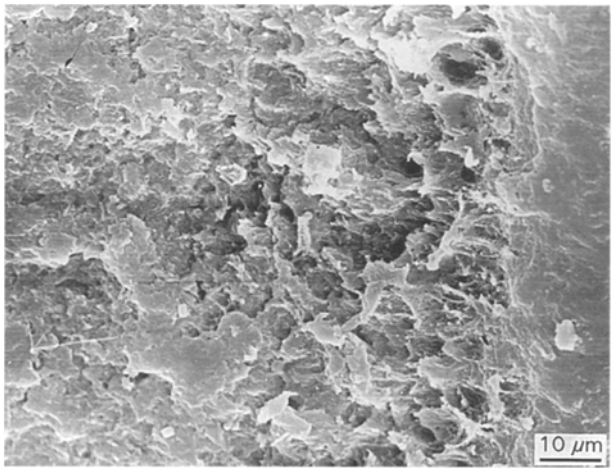

Figure 27 SEM micrograph of the fracture surface of material B fractured in air at +23 °C. The artificial notch is on the right side of the picture, the crack propagates from right to left.

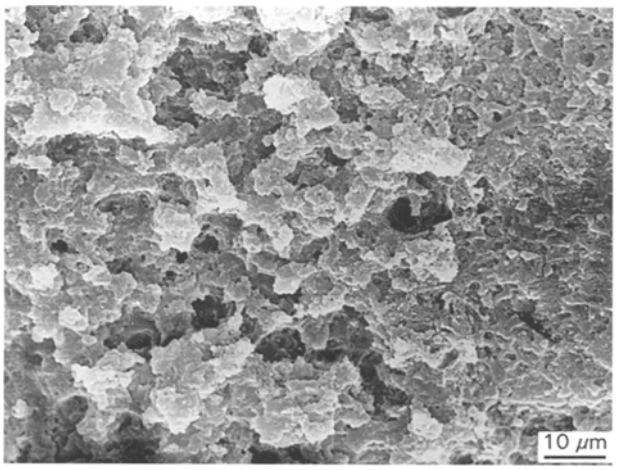

Figure 28 SEM micrograph of the fracture surface of material B fractured in CP at +23 °C. The artificial notch is on the right side of the picture, the crack propagates from right to left.

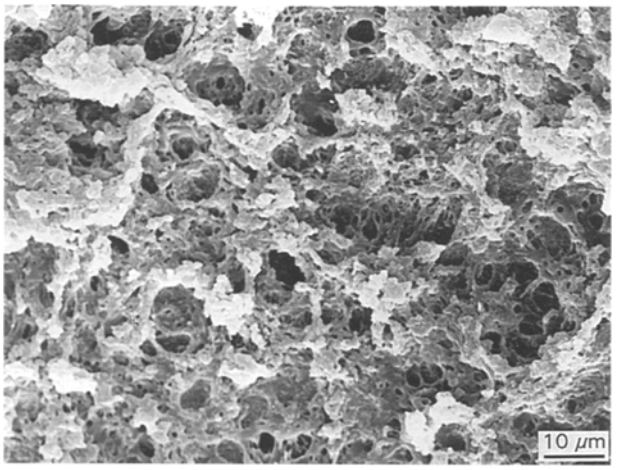

Figure 29 SEM micrograph of the fracture surface of material B fractured in F11 at +23 °C. The observed zone is near to the original notch, the crack propagates from right to left.

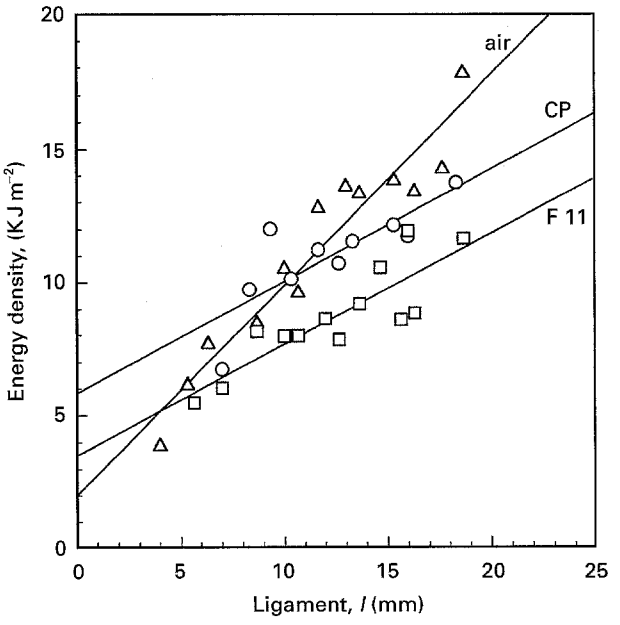

Figure 30 Plot of the energy density, $W_f/(l \times B)$, versus the ligament, l, for material B at a temperature of −23 °C in air (△), in liquid CP (○) and in liquid F11 (□). The solid lines represent linear regressions.

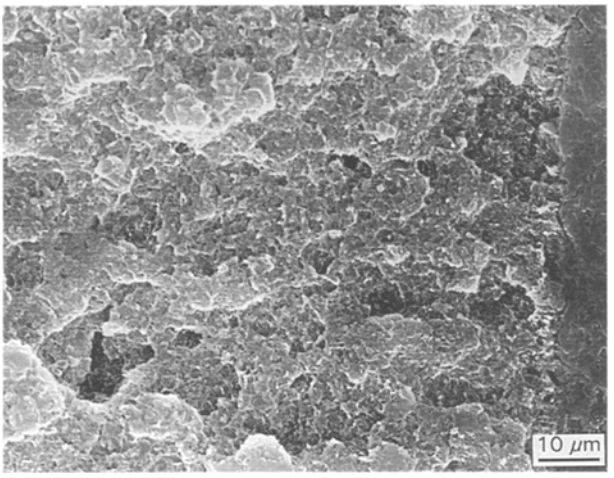

Figure 31 SEM micrograph of the fracture surface of material B fractured in air at −23 °C. The artificial notch is on the right side of the picture, the crack propagates from right to left.

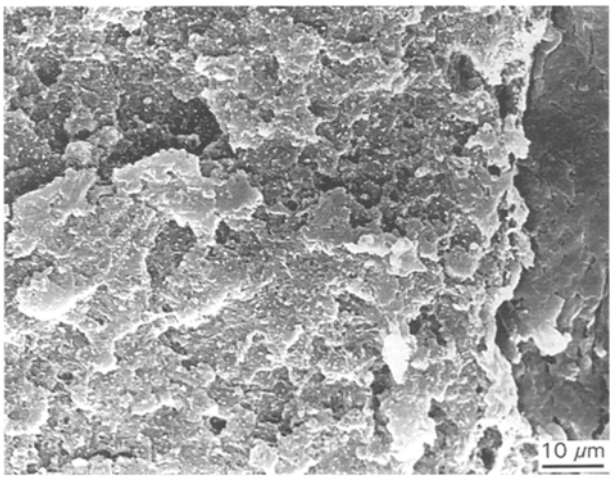

Figure 32 SEM micrograph of the fracture surface of material B fractured in CP at −23 °C. The artificial notch is on the right side of the picture, the crack propagates from right to left.

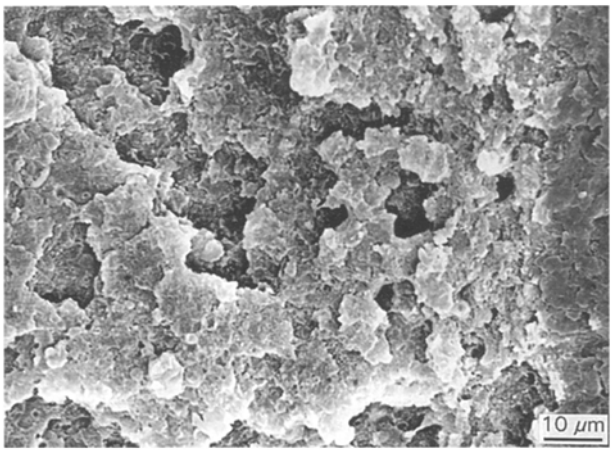

Figure 33 SEM micrograph of the fracture surface of material B fractured in F11 at −23 °C. The artificial notch is on the right side of the picture, the crack propagates from right to left.

The presence of an active plastic mechanism in the air fractured samples seems to be contradicted by the data reported in Fig. 18. However, a plastic zone for the sample fractured in air, since it can present a rectangular shape that does not vary its height with the ligament, can still exist, whilst no plastic deformation is observable in the specimen exposed to the liquid agents.

TABLE III Paris coefficients (from Equation 9 in the text) for the SCP tests performed in the present work. Due to the power nature of the Paris law, A and m have variable dimensions. The obtained values are for the stress intensity factors in MPa $m^{1/3}$ and for the crack speeds in m s^{-1}. The data in parenthesis relate to plasticized specimens

Material/aggressive agent	Pressure ($\times 10^2$ Pa)	A	m
A		7.6×10^{-14}	20.37
A/CP	100	1.9×10^{-13}	20.06
A/CP	160	1.6×10^{-12}	18.50
A/CP	200	(4.8×10^{-12})	(18.33)
A/F11	160	1.0×10^{-13}	20.64
A/F11	300	1.4×10^{-12}	18.56
A/F11	450	1.7×10^{-12}	19.52
A/F11	600	(4.9×10^{-11})	(17.58)
B		8.3×10^{-16}	23.93
B/CP	100	1.0×10^{-13}	19.92
B/CP	160	3.2×10^{-13}	19.60
B/CP	200	(5.6×10^{-13})	(20.43)
B/F11	160	2.3×10^{-14}	21.54
B/F11	300	2.7×10^{-13}	20.02
B/F11	450	1.5×10^{-12}	18.55
B/F11	600	(7.4×10^{-12})	(18.67)

Fig. 26 is a plot of the energy density versus the ligament for material B fractured in air, CP and F11 at +23 °C. An analysis of the figure demonstrates that, in this case, the presence of the aggressive agent does not cancel the plastic mechanisms inside the material and that, again, the energy density for fracture is higher for CP than for F11. The SEM survey is in agreement with the mechanical tests, showing an attack that can be defined as medium for CP and medium-strong for F11 (Figs 27–29). Also a visual analysis reveals a well defined plastic zone for all specimens, including those fractured in the presence of the agents.

Fig. 30 is a plot of the energy density versus the ligament for material B fractured in air, CP and F11 at −23 °C. In this case the situation is similar to the one described at +23 °C: the plastic mechanism is active also in the presence of the aggressive agents and the fracture energy density is higher for CP. The SEM analysis confirms that the attack of the solvents is very low or null (Figs 31–33).

In conclusion, the situation of the ESC in the presence of liquid agents is outlined in Table IV.

6. Conclusions

We summarize here the main conclusions of the present work:

Surface damage:

1. The formation of blisters on the HIPS panels of refrigerators is, according to our analysis, due to the pasticization of the PS matrix and to the subsequent micro blow-moulding produced by the thermal expansion of the blowing agent which is concomitant

TABLE IV Observation summary of the ESC behaviour in the presence of liquid aggressive agents. The symbols w_e and $w_p\gamma$ come from Equation 10 in the text

+23 °C	w_e (KJ m^{-2})	$w_p\gamma$ (KJ m^{-3})	Surface damage	Plastic zone shape
material A air	4.8	3.3×10^{-4}	–	ellipse
material A CP	0.3	5.3×10^{-5}	strong	none
material A F11	1.0	4.0×10^{-5}	strong	none
material B air	4.6	4.3×10^{-4}	–	ellipse
material B CP	5.1	2.3×10^{-4}	medium	ellipse
material B F11	1.3	4.3×10^{-4}	medium-strong	ellipse
−23 °C	w_e (KJ m^{-2})	$w_p\gamma$ (KJ m^{-3})	Surface damage	Plastic zone shape
material A air	3.8	5.8×10^{-4}	–	rectangle
material A CP	3.8	3.6×10^{-5}	medium	none
material A F11	2.0	1.4×10^{-5}	strong	none
material B air	2.0	7.9×10^{-4}	–	reduced ellipse
material B CP	5.8	4.2×10^{-4}	low	reduced ellipse
material B F11	3.5	4.2×10^{-4}	low	rectangle

to the thermal treatments that simulate the storing periods.

2. The examination of the solubility isotherm curve for the two systems: CP–PS and F11–PS, suggests that CP could behave more critically than F11. In fact, if we consider a condition of equal pressure, the amount of CP dissolved in the PS matrix is greater than for F11; moreover the lowering of T_g and the consequent plasticization results are again more significant in the CP case.

3. The presence of AN in the HIPS matrix can avoid the blistering problem due to the lower permeability to the blowing agents;

ESC in a gas:

1. A fracture mechanics test (slow crack propagation) in a gaseous environment demonstrated that the material B (containing AN) has a greater ESC resistance to the aggressive agents (CP and F11).

2. In a condition of equal pressure and equal stress intensity factor, the crack speed is higher in presence of gaseous CP than in the presence of F11.

3. In a condition of equal thermodynamic activity and equal stress intensity factor, there is no meaningful difference in the crack speed in the presence of the two gaseous agents;

ESC in a liquid:

1. A fracture mechanics test (essential work of fracture) in a liquid environment demonstrated again that the material B (containing AN) has a greater ESC resistance to the aggressive agents (CP and F11).

2. At the two tested temperatures (+23 °C and −23 °C), the effects of CP on the two HIPS materials appear, in this case, less damaging than those produced by F11.

Acknowledgements

L. Castellani, L. Bonifaci, M. Merlotti, M. Vighi, W. Ghizzi and F. Concetti are warmly acknowledged for their kind assistance and collaboration.

References

1. M. D. LEMONICK, *Time Int.* **45** (1994) 61.
2. R. A. BUBECK, C. B. ARENDS, E. L. HALL and J. B. VANDER SANDE, *Polym. Engng. Sci.* **21** (1981) 624.
3. S. V. HOA, *ibid.* **20** (1980) 1157.
4. A. SAVADORI, D. BACCI and C. MAREGA, *Polym. Test.* **7** (1987) 59.
5. M. A. VUL'F, V. S. POLONSKII, T. G. SHLYAKHOVA and Y. V. NIKITIN, *Int. Polym. Sci. Tech.* **15** (1988) T/62.
6. G. CIGNA, M. ROSSI, *Montedipe Internal Report 68/82* (1982).
7. Italian Patent 19 220 (1980).
8. Fed. Rep. Germ. Patent 2946 761 (1979).
9. Fed. Rep. Germ. Patent 2951 117 (1979).
10. Arbeits Gemelnschaft Kalteindustrie, *Prüf. Thermoplast. Kunst.* **31** (1970).
11. C. MAREGA, Zanussi Elettrodomestici SpA, private communication.
12. P. J. FLORY, "Principles of Polymer Chemistry" (Cornell University Press, Ithaca, NY, 1953).
13. A. F. M. BARTON, "CRC handbook of solubility parameters and other cohesion parameters" (CRC Press Inc., Boca Raton, Florida, 1983).
14. Y. W. MAI, *J. Mater. Sci.* **21** (1986) 904.
15. T. S. CHOW, *Macromolecules* **13** (1980) 362.
16. G. BROWN and A. J. KOVACS, in Proc. Conf. on Physics of Non-Crystalline Solids, 1965, edited by J. A. Prins (North-Holland, Amsterdam, 1965) p. 303.
17. G. F. SMITHS and J. A. THOEN, *J. Cellular Plastics* **29** (1993) 57.
18. J. G. WILLIAMS and M. J. CAWOOD, *Polym. Test.* **9** (1990) 15.
19. European group on fracture, *EGF Newslett.* **1** (1986/1987).
20. C. MAESTRINI, L. MONTI and H. H. KAUSCH, *Polymer* (accepted).
21. P. C. PARIS, in Proc. 10th Sagamore Conf., 1964 (Syracuse University Press, Syracuse, NY, 1964).
22. R. W. HERTZBERG and J. A. MANSON, "Fatigue of Engineering Plastics" (Academic Press, London, 1980).
23. R. W. HERTZBERG and J. A. MANSON, in "Encyclopaedia of Polymer Science and Engineering", 1985 (John Wiley and Sons, New York, 1985) vol. 10.
24. B. COTTERELL and J. K. REDDEL, *Int. J. Fract.* **13** (1977) 267.
25. K. B. BROBERG, *ibid.* **4** (1968) 11.
26. Y. W. MAI and B. COTTERELL, *ibid.* **32** (1986) 105.
27. Y. W. MAI, B. COTTERELL, R. HORLYCK and G. VIGNA, *Polym. Engng. Sci.* **27** (1987) 804.
28. Y. W. MAI and P. POWELL, *J. Polym. Sci. B: Polym. Phys.* **29** (1991) 785.

29. C. A. PATON and S. HASHEMI, *J. Mater. Sci.* **27** (1992) 2279.
30. J. G. WILLIAMS, "Fracture Mechanics of Polymers" (Ellis Horwood, Chichester, 1984).
31. C. MAESTRINI, M. MERLOTTI, M. VIGHI and E. MALAGUTI, *J. Mater. Sci.* **27** (1992) 5994.
32. S. ANZALDI, L. BONIFACI, E. MALAGUTI, M. VIGHI and G. P. RAVANETTI, *J. Mater. Sci. Lett.* **13** (1994) 1555.
33. K. KATO, *Polym. Engng. Sci.* **7** (1967) 38.
34. E. J. KRAMER, in "Developments in Polymer Fracture", edited by E. H. Andrew (Applied Science, London, 1979).
35. H. G. OLF and A. PETERLIN, *J. Polym. Sci.: Polym. Phys.* **12** (1974) 2209.
36. N. BROWN, *J. Macromol. Sci.-Phys.*, **B19** (1981) 387.

Received 6 March 1995
and accepted 15 January 1996